Electronic Supplementary Material (ESI) for Journal of Materials Chemistry A.

Supplementary Materials for

3D Bridge-Arch Structured Dual-Sided Evaporator for Practical-Level, All Weather Water Harvesting and Desalination

Meijie Chen[1,*], Shuang Li[1], Xingyu Chen[1], Yimou Huang[1], Bin Liu[1], Hongjie Yan[1], Brian W. Sheldon[2], Qing Li[1,*], Changmin Shi[2,*]

[1] School of Energy Science and Engineering, Central South University, Changsha 410083, China

[2] School of Engineering, Brown University, Providence 02912, Rhode Island, USA.

* Corresponding Author. chenmeijie@csu.edu.cn (M. Chen); qingli@csu.edu.cn (Q. Li), changmin_shi@brown.edu (C. Shi)

This PDF file includes:

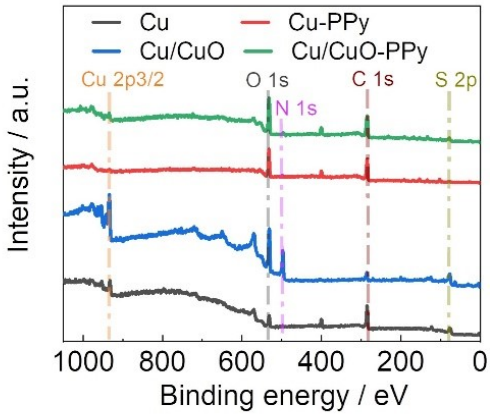

Fig. S1. XPS spectra of different samples.

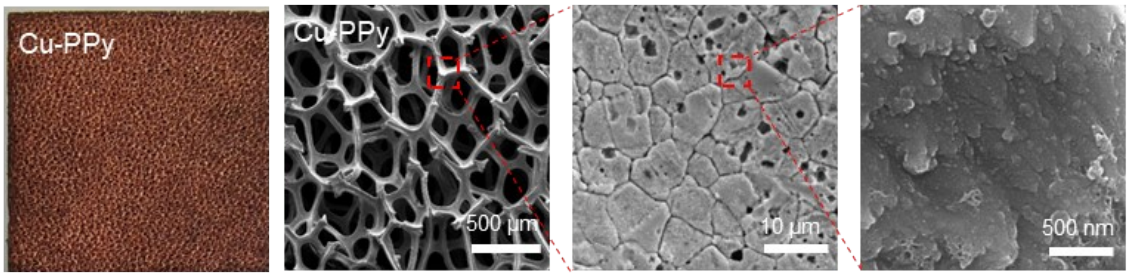

Fig. S2. Optical picture and SEM images of the Cu-PPy foam.

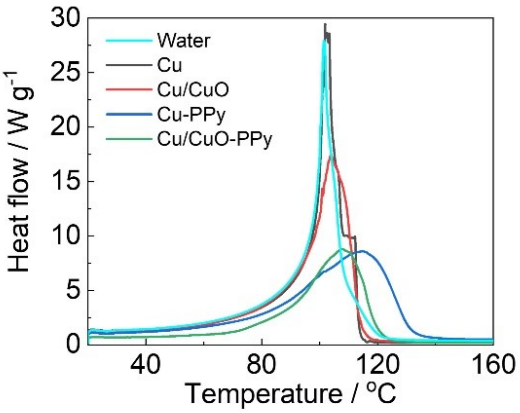

Fig. S3. Differential scanning calorimetry curves of water in Cu foam, Cu/CuO foam, Cu-PPy foam, Cu/CuO-PPy foam, and pure water.

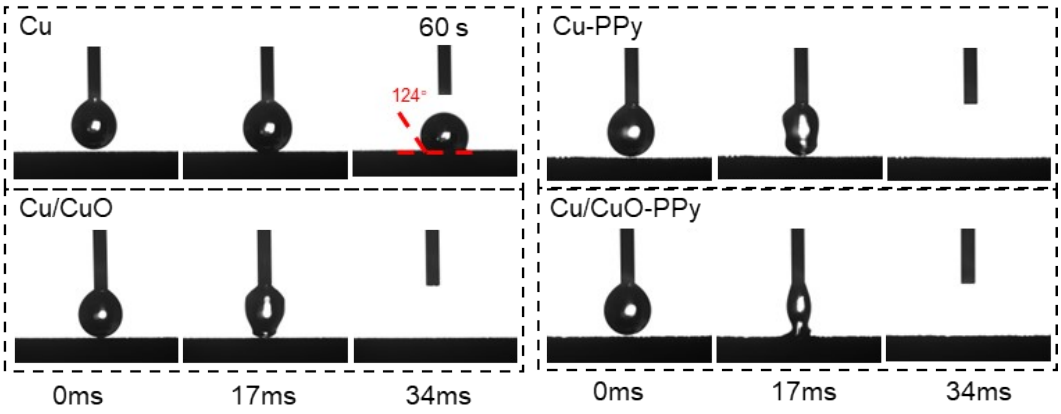

Fig. S4. Water contact angle variations of different samples.

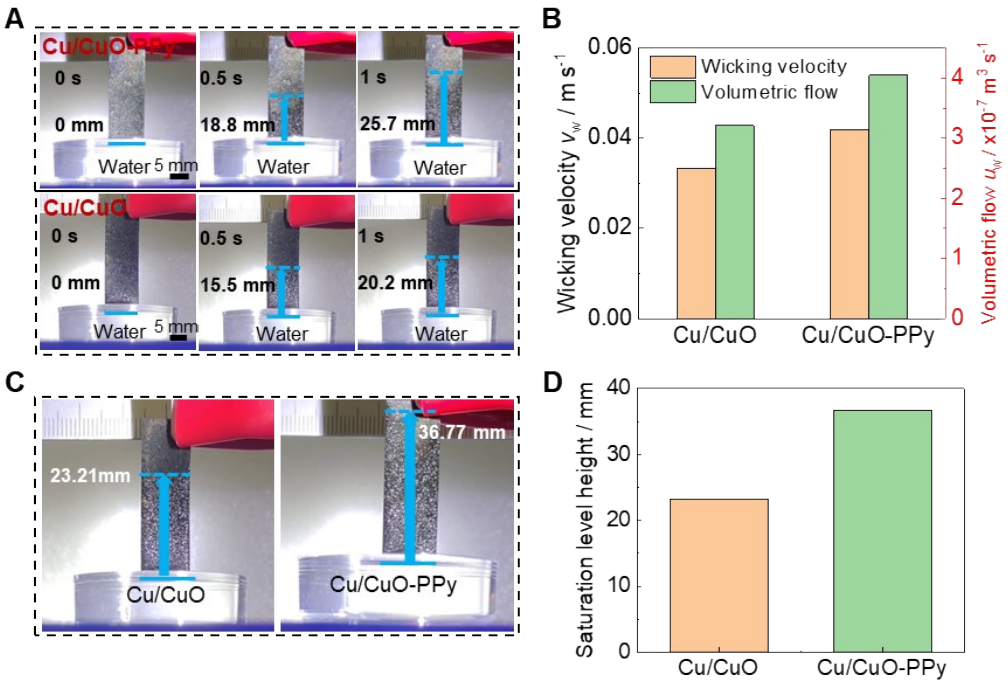

Fig. S5. Liquid supply (wicking) capability of Cu/CuO foam and Cu/CuO-PPy foam wicking structures. (**A**) Snapshots of wicking experiments on Cu/CuO foam, and Cu/CuO-PPy foam. The wicking front is marked by the blue dashed lines; (**B**) Average wicking velocity v_w and volumetric flow rate u_w on the Cu/CuO foam and Cu/CuO-PPy foam; (**C**) Photos of Cu/CuO foam and Cu/CuO-PPy foam when the water level reaches a stable state; (**D**) Saturation level height of Cu/CuO foam and Cu/CuO-PPy foam.

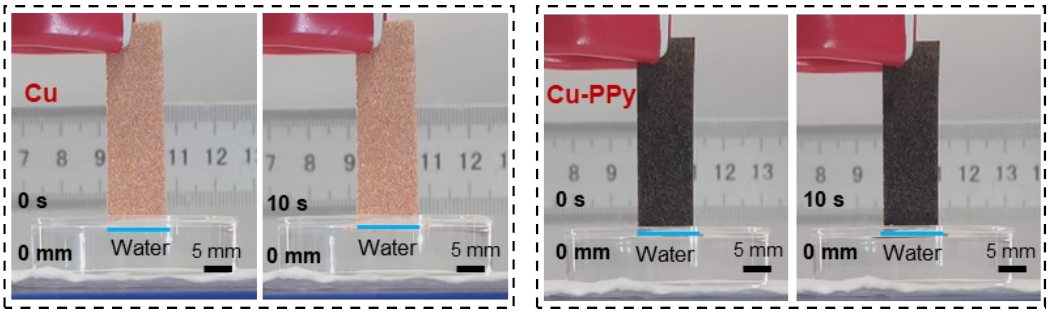

Fig. S6. Optical picture of Cu and Cu-PPy foam inserted into water reservoir for water supply against gravity.

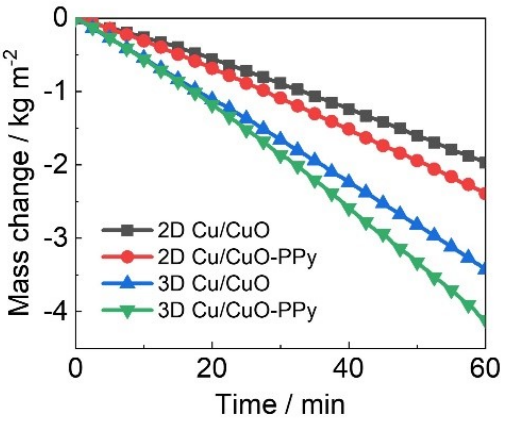

Fig. S7. Mass change curves of the 2D Cu/CuO foam, 2D Cu/CuO-PPy foam, 3D Cu/CuO foam, and 3D Cu/CuO-PPy foam evaporation systems under 1 sun.

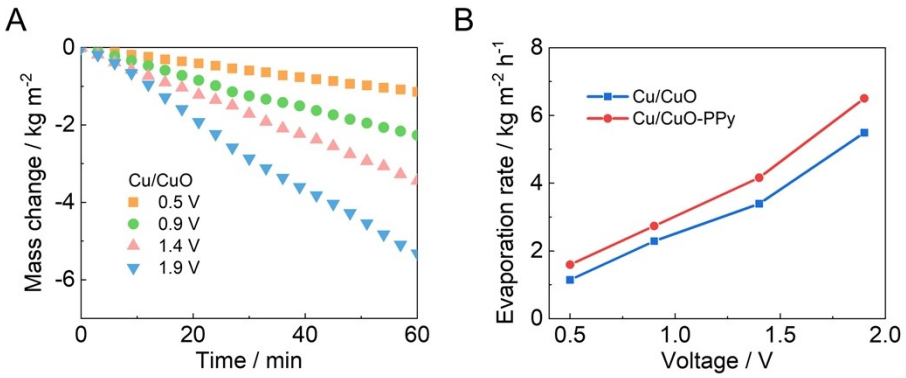

Fig. S8. Evaporation performance of 3D Cu/CuO evaporators driven by Joule heating at different voltages. (**A**) Mass changes. (**B**) Evaporation rates.

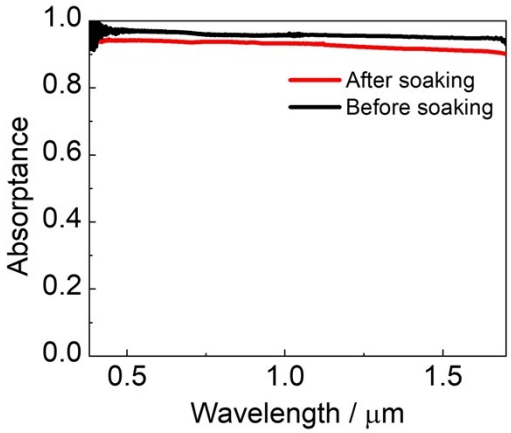

Fig. S9. Spectral absorptance of Cu/CuO-PPy foam before and after soaking in 10 wt.% brine for 12 h.

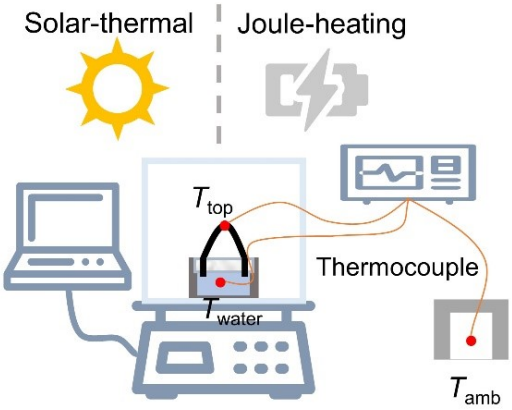

Fig. S10. Schematic diagram of outdoor experiment setup.

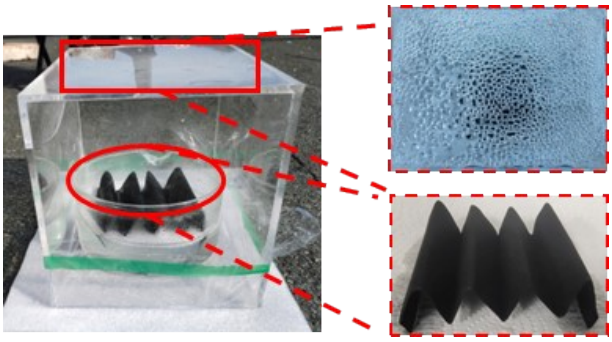

Fig. S11. Experimental setups for outdoor water yield performance evaluation.

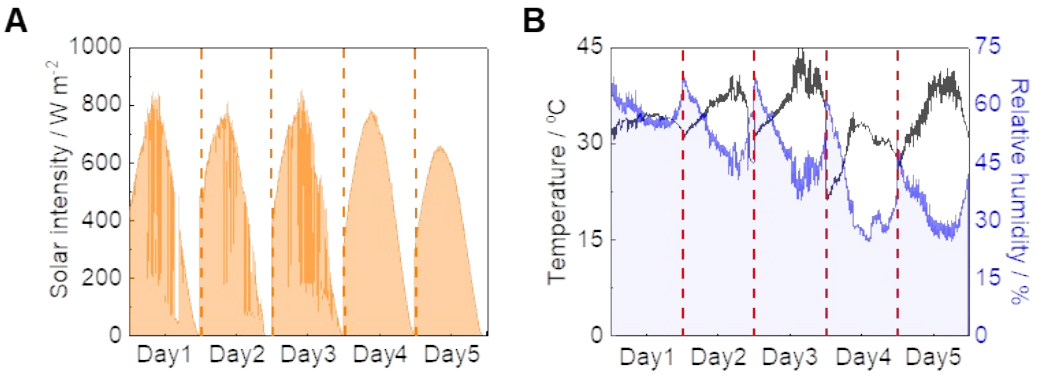

Fig. S12. Environmental conditions during the outdoor experiment. (**A**) Solar intensity and (**B**) ambient temperature and relative humidity for a 5-day outdoor experiment.

Table S1. Summary of water evaporation performance under one sun illumination.

Evaporator	T_{amb} (°C)	RH (%)	Structure	Rate (kg m^{-2} h^{-1})	Ref.
Aerogels loaded with gold nanoparticles	22	55	2D	2.7	(*1*)
Membrane assembled from copper-zinc-tin-selenide nano-carambolas	25	30~40	2D	1.5	(*2*)
Bridge evaporator by paper and wood frame	23~25	60~70	3D	1.64	(*3*)
1D-*O*-doped MoS_{2-x} nanosheet assembly	28	40	1D	2.5	(*4*)
3D cup-shaped evaporator with $CuFeMnO_4$	21.5	55	3D	2	(*5*)
Janus evaporator by hydroxyapatite nanowires and nickel oxide	28	40	2D	1.38	(*6*)
3D evaporator coated with carbon black	24	35	3D	1.6	(*7*)
Maize straw/graphene aerogels	25	50	3D	3.2	(*8*)
Vertically aligned graphene pillar array	25	20	3D	2.1	(*9*)
Carbonaceous nanosheets/MXene hybrid foam	25~26	55~60	3D	1.4	(*10*)
Zeolitic imidazolate framework-isolated graphene	/	/	2D	1.8	(*11*)
Nanostructured Ni–NiO_x/Ni foam	15~18	18~20	2D	1.4	(*12*)
Cu/CuO-PPy foam	**24~26**	**55~65**	**3D**	**4.1**	**This work**

Note S1: Heat loss calculation

The heat loss of the evaporation system consists of radiation loss, conduction loss, and convective loss, which are analyzed as follows (*3*, *13–15*):

(1) Radiation loss

The radiation loss can be calculated by the Stefan-Boltzmann law:

$$\phi = \varepsilon A\sigma\left(T_1^4 - T_2^4\right)$$

where Φ is the heat flux, ε is the emissivity of Cu/CuO-PPy foam (0.86), A is the evaporation surface area, σ is the Stefan-Boltzmann constant (5.67×10^{-8} W m^{-2} k^{-4}), and T_1 is the temperature of the absorber under 1 kW m^{-2} solar illumination (308 K). T_2 is the atmospheric temperature (298 K), and the calculated radiation loss is ~5.4%.

(2) Conduction loss

The conduction loss can be obtained by the following formula:

$$Q = Cm\Delta T$$

where Q is the heat energy, C is the specific heat capacity of water (4.2 J g^{-1} ℃$^{-1}$), m is the volume weight of water (20 g), and ΔT is the temperature change (1.5℃) after evaporation for 1 h. Therefore, the calculated thermal conductivity loss is ~ 3.0%.

(3) Convection loss

The convection loss can be obtained by the following formula:

$$\phi = hA\Delta T$$

where Φ is the heat flux, h is the convective heat transfer coefficient (5 W m^{-2} K^{-1}), A is the evaporation surface area, ΔT is the temperature difference between the Cu/CuO-PPy foam surface and the surrounding environment (10 K). Thus, the calculated convection loss is ~ 5.0%.

Based on the above analysis, the radiation loss, conduction loss, and convection loss are calculated to be 5.4%, 3.0%, and 5.0%, respectively. Under one sun, the total heat loss of the evaporation system is 13.4% and the solar-evaporation efficiency is 86.6%.

References

1. Z. Huang, S. Li, X. Cui, Y. Wan, Y. Xiao, S. Tian, H. Wang, X. Li, Q. Zhao, C.-S. Lee, Broadband aggregation-independent plasmonic absorber for highly efficient solar steam generation. *Journal of Materials Chemistry A* **8**, 10742–10746 (2020).
2. Y. Yang, W. Que, J. Zhao, Y. Han, M. Ju, X. Yin, Membrane assembled from anti-fouling copper-zinc-tin-selenide nanocarambolas for solar-driven interfacial water evaporation. *Chemical Engineering Journal* **373**, 955–962 (2019).
3. Y. Luo, S. Fei, W. Xiu-Li, W. Yu-Zhong, Water bridge solar evaporator with salt-resistance and heat localization for efficient desalination. *Journal of Materials Chemistry A* **11**, 3118–3125 (2023).
4. Q. Lu, W. Shi, H. Yang, X. Wang, Nanoconfined Water-Molecule Channels for High-Yield Solar Vapor Generation under Weaker Sunlight. *Advanced Materials* **32**, 1–7 (2020).
5. Y. Shi, R. Li, S. Hong, Y. Shi, R. Li, Y. Jin, S. Zhuo, L. Shi, J. Chang, S. Hong, A 3D Photothermal Structure toward Improved Energy Efficiency in Solar Steam Generation. *Joule* **2**, 1171–1186 (2018).
6. D. Qin, Y. Zhu, R. Yang, Z. Xiong, A salt-resistant Janus evaporator assembled from ultralong hydroxyapatite nanowires and nickel oxide for efficient and recyclable solar desalination. *NANOSCALE* **12**, 6717–6728 (2020).
7. X. Li, J. Li, J. Lu, N. Xu, C. Chen, X. Min, B. Zhu, H. Li, L. Zhou, S. Zhu, T. Zhang, J. Zhu, Enhancement of Interfacial Solar Vapor Generation by Environmental Energy Enhancement of Interfacial Solar Vapor Generation by Environmental Energy. *Joule* **2**, 1331–1338 (2018).
8. Y. Kong, H. Dan, W. Kong, Y. Gao, Y. Shang, K. Ji, Q. Yue, B. Gao, Self-floating maize straw/graphene aerogel synthesis based on microbubble and ice crystal templates for efficient solar-driven interfacial water evaporation. *Journal of Materials Chemistry A* **8**, 24734–24742 (2020).

9. P. Zhang, Q. Liao, H. Yao, H. Cheng, Y. Huang, C. Yang, L. Jiang, L. Qu, Three-dimensional water evaporation on a macroporous vertically aligned graphene pillar array under one sun †. *Journal of Materials Chemistry A* **6**, 15303–15309 (2018).

10. X. Fan, Y. Yang, X. Shi, Y. Liu, H. Li, J. Liang, Y. Chen, A MXene-Based Hierarchical Design Enabling Highly Efficient and Stable Solar-Water Desalination with Good Salt Resistance. *Advanced Functional Materials* **30**, 1–11 (2020).

11. X. Han, L. V Besteiro, C. Sher, L. Koh, H. K. Lee, I. Y. Phang, G. C. Phan-quang, J. Y. Ng, H. Yi, F. Sim, C. L. Lay, A. Govorov, X. Y. Ling, Intensifying Heat Using MOF-Isolated Graphene for Solar-Driven Seawater Desalination at 98% Solar-to-Thermal Efficiency. *Advanced Functional Materials* **31**, 1–7 (2021).

12. D. Wu, D. Qu, W. Jiang, G. Chen, C. Zhuang, Z. Sun, L. An, Self-floating nanostructured Ni–NiOx/Ni foam for solar thermal water evaporation. *Journal of Materials Chemistry A* **7**, 8485–8490 (2019).

13. Y. Guo, Y. Sui, J. Zhang, Z. Cai, B. Xu, An all-day solar-driven vapor generator via photothermal and Joule-heating effect. *Journal of Materials Chemistry A* **8**, 25178–25186 (2020).

14. H. Wang, R. Zhang, D. Yuan, S. Xu, L. Wang, Gas Foaming Guided Fabrication of 3D Porous Plasmonic Nanoplatform with Broadband Absorption , Tunable Shape , Excellent Stability , and High Photothermal Efficiency for Solar Water Purification. *Advanced Functional Materials* **30**, 1–8 (2020).

15. C. Wang, K. Xu, G. Shi, D. Wei, Water Skin Effect and Arched Double-Sided Evaporation for Boosting All-Weather High Salinity Desalination. *Advanced Energy Materials* **13**, 2300134 (2023).